JOURNAL OF PHYSICAL CHEMISTRY A (ISSN: 1089-5639) 118: p. 5238. (2014)
DOI: 10.1021/jp504496k

Solvation and Protonation of Coumarin 102 in Aqueous Media - a Fluorescence Spectroscopic and Theoretical Study

Dóra Hessz,[§] Bence Hégely,[†] Mihály Kállay,[†] Tamás Vidóczy,[§] Miklós Kubinyi*[§,#]

[§] Institute of Materials and Environmental Chemistry, Research Center for Natural Sciences, Hungarian Academy of Sciences, 1519 Budapest, P.O. Box 286., Hungary

[†]MTA-BME Lendület Quantum Chemistry Research Group, Department of Physical Chemistry and Material Science, Budapest University of Technology and Economics, 1521 Budapest, Hungary

[#] Department of Physical Chemistry and Materials Science, Budapest University of Technology and Economics, 1521 Budapest, Hungary

ABSTRACT

The ground and excited state protonation of Coumarin 102 (C102), a fluorescent probe applied frequently in heterogeneous systems with an aqueous phase, has been studied in aqueous solutions by spectroscopic experiments and theoretical calculations. For the dissociation constant of the protonated form in the ground state, $pK_a = 1.61$ was obtained from the absorption spectra, for the excited state dissociation constant $pK_a^* = 2.19$ was obtained from the fluorescence spectra. These values were closely reproduced by theoretical calculations via a thermodynamic cycle – the value of pK_a^* also by calculations via the Förster cycle - using an implicit-explicit solvation model (polarized continuum model + addition of a solvent molecule). The theoretical calculations indicated that (i) in the ground state C102 occurs primarily as a hydrogen bonded water complex, with the oxo group as the binding site, (ii) this hydrogen bond becomes stronger upon excitation; (iii) in the ground state the amino nitrogen atom, in the excited state the carboxy oxygen atom is the protonation site. A comprehensive analysis of fluorescence decay data yielded the values $k_{pr} = 3.27\times10^{10}$ M^{-1} s^{-1} for the rate constants of excited state protonation, and $k_{dpr} = 2.78\times10^{8}$ s^{-1} for the rate constant of the reverse process (k_{pr} and k_{dpr} were treated as independent parameters). This, considering the relatively long fluorescence lifetimes of neutral C102 (6.02 ns) and its protonated form (3.06 ns) in aqueous media, means that a quasi-equilibrium state of excited state proton transfer is reached in strongly acidic solutions.

KEYWORDS

fluorescent dye probe, specific solute-solvent interactions, excited state proton transfer, TD-DFT method, Coumarin 480

1. INTRODUCTION

7-amino-coumarins are versatile fluorescent probes.[1] Their S_0-S_1 excitation is of charge transfer character, making them sensitive to the polarity of their local environment. Besides, since their carbonyl group is a hydrogen bond acceptor site, whereas their amino group can act both as a hydrogen bond donor and as a hydrogen bond acceptor site, 7-amino-coumarins also provide information on the hydrogen bonding ability of the medium.

A significant representative of these dyes is Coumarin 102 (C102, Coumarin 480). The fixation of its amino group to the benzene moiety prevents the formation of a twisted intramolecular charge-transfer (TICT) excited state, which contributes to the deactivation of coumarins with unfixed amino groups.[2,3] As a rigid rotor solute, it is suitable to probe the local friction via measuring the decay of fluorescence anisotropy.[4]

It is used as a model drug for studying drug-protein interactions[5,6] and for testing drug delivery systems (micelles,[7-9] liposomes,[10] microcapsules,[11] polymeric core-shell assemblies[12]). Inserting C102 in DNA-s, the internal dynamics of DNA chains can be studied.[13,14] As a weak base, C102 is protonated in strongly acidic media, which has been utilized to probe the local acidity in proton-transfer membranes[15,16] and at water-micelle interfaces.[17] Motivated by such applications of the dye, which concern aqueous solutions or heterogeneous systems with an aqueous phase, our aim in the present study has been to describe the solvation and protonation of C102, as two essential interactions occurring in the aqueous solutions of the dye.

The impact of hydrogen bonds on the photophysical properties of C102 has been studied primarily in organic media. The variation of its absorption and fluorescence band maxima in neat solvents, as a function of the Kamlet-Taft parameter, indicated that C102 is a much stronger hydrogen bond acceptor in its S_1 state than in its ground state.[18] In the presence of aliphatic alcohols[18,19] and phenol[20] its fluorescence band shows a much stronger red shift than its absorption band and there is a delay period in its fluorescence decay curve, which can be explained in terms of the increased stability of the hydrogen bonded solute-solvent complexes. As was shown by time-resolved fluorescence anisotropy measurements, the rotational dynamics of C102 in trichloro-ethanol could be described as the rotation of a solute-solvent complex following the hydrodynamic model with slip conditions.[21] Time-resolved vibrational spectroscopic experiments on the hydrogen bonded complexes of C102 with phenol,[22,23] aniline[24] and water[25] indicated the cleavage of the hydrogen bonds in a few hundred femtoseconds

following the $S_0 \rightarrow S_1$ excitation of C102. Theoretical calculations, however, indicated the initial strengthening of hydrogen bonds in these complexes after the excitation of the dye molecule.[26-29]

Excited state proton transfer of C102 was observed in the acidic aqueous[30] and ethanol[31] solutions of the dye. It was manifested as a stretch of the rising edge of the fluorescence decay curves measured in the emission wavelength range of the protonated species.

In this study we endeavored to theoretically explain the absorption and fluorescence spectra of C102 measured at different pH values, with special regard to the effect of the water complexes and the protonation in the ground and first excited state on its spectral properties.[30,32] The theoretical calculations are especially important for the understanding of the excited state behavior of the molecule since the experimental mapping of the deactivation channels is hampered by the short lifetime of the first excited state.

The theoretical modeling of excited state processes in condensed phase, such as complex formation with the solvent molecules or proton transfer are challenging because particular species, e.g., hydroxonium ions, cannot be described by simple implicit solvation approaches and more sophisticated treatment of the solute-solvent interactions are required. For the quantitative description of the effect of the excited-state complexation and protonation two different approaches were invoked: the Förster cycle[33] and the thermodynamic cycle.[34,35] The Förster cycle is an indirect method, which uses the ground-state thermodynamic properties as well as the electronic transition energies of the protonated and non-protonated species for the estimation of the equilibrium constant of the excited-state acid-base equilibrium. Since the method neglects the molar entropy change due to the electronic excitation, its physical meaning is in question. Nevertheless, this simple approach provides a good estimate for the change in the basicity with respect to the ground state.[36] The thermodynamic cycle approach supposes an equilibrium state between the coumarin base and its conjugated acid (BH^+), and that the acid-base equilibrium can be characterized by the standard Gibbs energy of reaction of the protonation $(\Delta_r G^*_{aq})$ or the logarithmic acid dissociation constant (pK_a).

The interpretation of the excited-state logarithmic acidity constant (pK_a^*) is not straightforward, since an ensemble of electronically excited molecules is often far from thermodynamic equilibrium.[37] Even though the relaxation of the solvent and other phenomena, such as the excited-state proton transfer are extremely fast processes, due to the deactivation

channels the lifetime of the excited states can be short to reach thermodynamic equilibrium.[38] Consequently, the pK_a^* values, determined by the thermodynamic cycle approaches cannot be interpreted as a rigorous thermodynamic quantity, but as a qualitative measure of the excited state basicity. In order to assess to what extent the equilibrium state of solute-solvent proton transfer is reached following the excitation of C102, a comprehensive kinetic analysis of the fluorescence decay curves measured in acidic solutions has also been included in this study.

2. EXPERIMENTAL AND THEORETICAL METHODS

All the spectroscopic experiments were carried out at 25 °C. The UV-vis absorption spectra were recorded on an Agilent 8453 diode array spectrometer. The steady state fluorescence spectra and fluorescence decay curves were measured on an Edinburgh Instruments FLSP920 combined steady state and lifetime spectrometer, which uses the method of time correlated single photon counting for measuring the fluorescence decay. The excitation light source was a Xe900 steady state arc lamp when measuring the fluorescence spectra, and an EPL 375 picosecond pulsed diode laser when the fluorescence decay curves were recorded. This diode laser emitted pulses of 130 ps FWHM (full width at half maximum) at 378 nm.

C102 was obtained from Exciton and was used without further purification. The hydrochloric acid (37%, analytical grade) was purchased from Carlo Erba Reagents. The instrument response function (IRF) was determined by scattering method using Ludox HS-30 (purchased from Sigma Aldrich).

The ground- and excited-state Gibbs energies as well as electronic transition energies required for the above cycles were computed with the Gaussian09 suite.[39] The ground-state properties were calculated with aid of density functional theory (DFT)[40,41] using the PBE0 exchange-correlation hybrid functional[42] and the 6-311++G** [43] basis set. For the excited states we chose the time-dependent DFT model (TDDFT)[44] with the same functional and basis set. For the description of the solvent effect in the condensed phase, both in the ground and excited states, the SMD[45] solvation model of Truhlar and co-workers were employed (in the following referred to as implicit model or *Imp* for short), which is based on the conductor polarized continuum model (CPCM).[46,47] According to previous studies, the PCM approaches satisfactorily describe

the electrostatic effect of water molecules on solutes similar to C102[48], while the SMD method is widely used for systems dominated by non-electrostatic interactions[49] and frequently applied to the calculation of ground-state pK_a-s.[50] Two approaches of the CPCM solvation model were employed:[51] the equilibrium (*eq*) and the non-equilibrium (*non-eq*) solvation, which take into account if the solvent molecules have enough time to reorient according to the electron density of the solute. In addition to the implicit approaches the specific solvent interactions in the aqueous solution were also modeled by adding an explicit water molecule (implicit-explicit or *Imp-Exp* approach). To simulate the hydrogen-bonded complexes in the solution the water molecule was placed to the oxo or amino group of the coumarin. Since the protonation of the molecule also takes place at those sites, the protonated coumarins were modeled by the corresponding species. The chemical structures of the model species considered and their notations are shown in Figure 1.

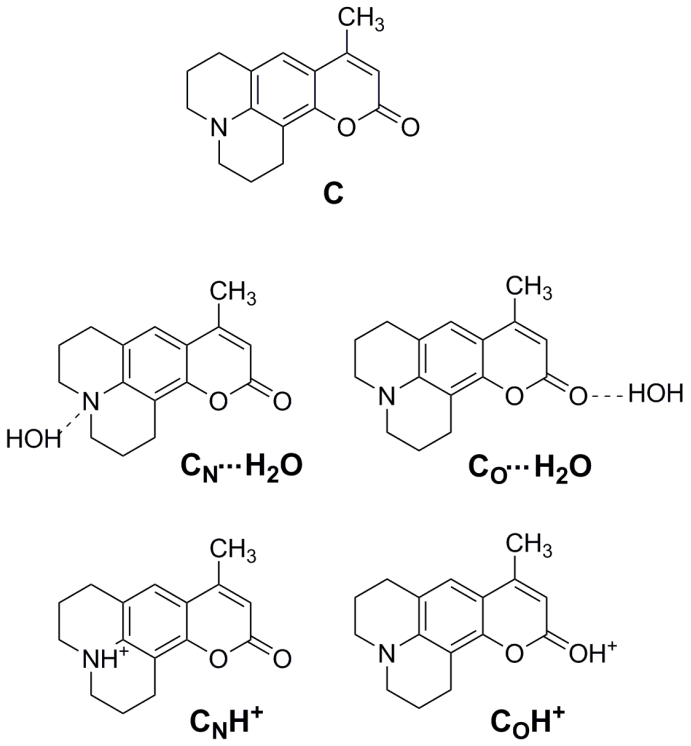

Figure 1. Structures of Coumarin 102 (C), its water complexes and protonated forms.

For the simulation of the experimental absorption spectra vertical excitation energies and oscillator strengths were computed at the optimized ground-state geometries. In the S_0 state the *eq* solvation model of the CPCM scheme were used, while in the S_1 state the *non-eq* solvation of state-specific (SS) CPCM approach was employed.[52] The essence of the SS procedure is that the electrostatic potential derived from the excited-state electron density is made self-consistent with the reaction field of the solvent continuum. The theoretical spectra calculated with the SS-CPCM approach are superior[52] to those obtained by the previously developed linear response CPCM (LR-CPCM) formalism,[53] which avoids the aforementioned relatively expensive iterative procedure. Nevertheless, the transitions to the higher excited states required for the simulation of the whole spectrum were treated with the LR-CPCM scheme since we are primarily interested in the $S_0 \rightarrow S_1$ transition. For the calculation of the fluorescence spectra a similar protocol was followed with the important difference that the optimized geometries of the S_1 state were used for the calculation of the emission energies and transition probabilities, and for the calculation of the energy of the S_1 state (S_0 state) the *eq* (*non-eq*) solvation of the SS-CPCM (CPCM) scheme was employed. For the spectrum simulations a Gauss function of 2000 cm^{-1} half width at half maximum was placed to the computed transition wavelengths. The heights of the functions were proportional to the calculated oscillator strengths and were rescaled in order for the function corresponding to the lowest transition to match the height of the corresponding experimental peak.

From the computed transition energies of the protonated and non-protonated species the excited state logarithmic acid dissociation constant, pK_a^*, was determined according to the Förster-cycle as[36]

$$pK_a^* = pK_a - N_A[(\Delta E_{abs,BH^+} + \Delta E_{em,BH^+})/2 - (\Delta E_{abs,B} + \Delta E_{em,B})/2]/\ln 10RT\,, \qquad (1)$$

where $\Delta E_{abs,BH^+}$ and $\Delta E_{em,BH^+}$ are, respectively, the absorption and emission energies of the protonated species, $\Delta E_{abs,B}$ and $\Delta E_{em,B}$ are the corresponding quantities for the non-protonated species, R is the universal gas constant, T is the temperature (298.15 K), N_A is the Avogadro constant (6.02×10^{23} 1/mol), and pK_a is the ground-state logarithmic acid dissociation constant. Though the latter quantity was also calculated using the thermodynamic cycle approach, to improve the accuracy of the computed pK_a^*, in the Förster-cycle the experimental value of pK_a was considered.

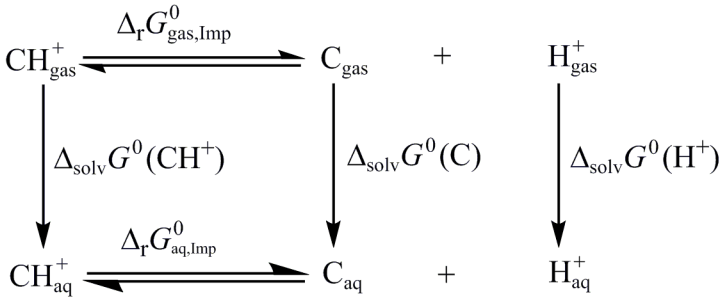

(a) Dissociation of protonated coumarin, using implicit solvation model.

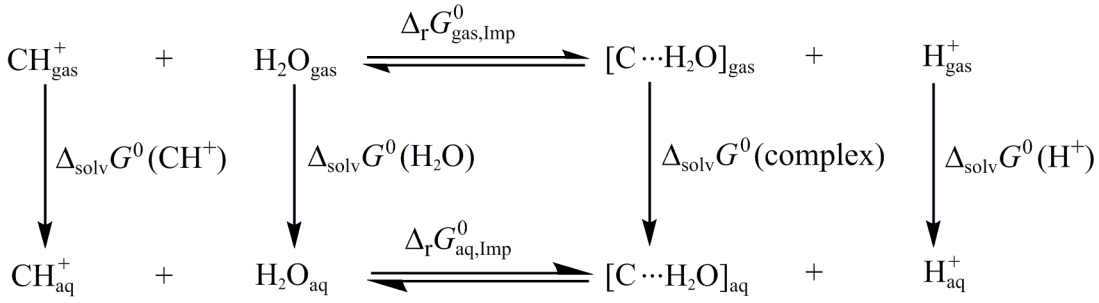

(b) Dissociation of protonated coumarin, using implicit-explicit solvation model.

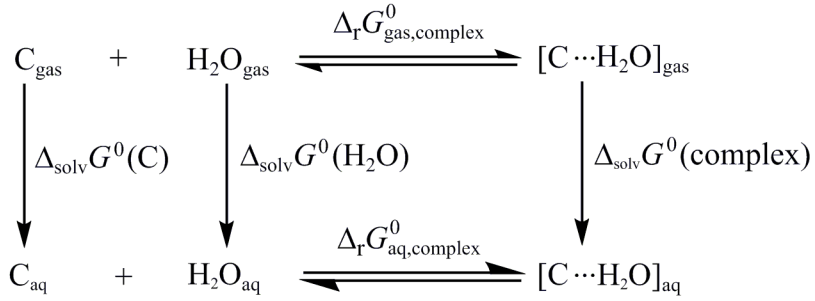

(c) Formation of coumarin-water complex.

Figure 2. Schemes of thermodynamic cycles applied in the theoretical calculations.

As mentioned above, the pK_a just as the Gibbs energies of reaction for the proton transfer and water complex formation were also determined from thermodynamic cycles, which are sketched in Figure 2. The effect of the solute-solvent interactions in the condensed phase on the protonation were considered both with the *Imp* (Figure 2a) and *Imp-Exp* (Figure 2b) models,

while thermodynamic quantities characterizing the formation of the complex were computed with the *Imp* approach (Figure 2c). The horizontal arrows represent the Gibbs energy of the gas- ($\Delta_r G^0_{gas,Imp}$, $\Delta_r G^0_{gas,Imp-Exp}$) and condensed-phase ($\Delta_r G^0_{aq,Imp}$, $\Delta_r G^0_{aq,Imp-Exp}$) protonation as well as that for the complex formation ($\Delta_r G^0_{gas,complex}$, $\Delta_r G^0_{aq,complex}$), while the vertical arrows stand for the Gibbs energy of solvation of the species [$\Delta_{solv} G^0(C)$, $\Delta_{solv} G^0(complex)$, $\Delta_{solv} G^0(H^+)$, $\Delta_{solv} G^0(CH^+)$, $\Delta_{solv} G^0(H_2O)$]. In the case of the *Imp* solvent model the ground-state Gibbs energy of acid dissociation in the aqueous solution can be expressed as

$$\Delta_r G^0_{aq} = \Delta_r G^0_{gas} - \Delta_{solv} G^0(\mathrm{CH^+}) + \Delta_{solv} G^0(\mathrm{C}) + \Delta_{solv} G^0(\mathrm{H^+}) \quad (2)$$

$$\Delta_r G^0_{gas} = -G^0_{gas}(\mathrm{CH^+}) + G^0_{gas}(\mathrm{C}) + G^0_{gas}(\mathrm{H^+}) \quad (3)$$

$$\Delta_{solv} G^0(X) = \left(E_{aq}(X) + G_{CDS}(X)\right) - E_{gas}(X) + \Delta G^0_{add}, \quad (4)$$

from which pK_a is obtained by the

$$pK_a = \Delta_r G^0_{aq} / \ln 10 RT \quad (5)$$

expression, where the symbols $G^0_{gas}(X)$ denote the gas-phase Gibbs energies of the species considered and the water molecule. The solvation Gibbs energies $\Delta_{solv} G^0(X)$ of the considered species *X* were calculated as defined in the SMD model: from the differences of $E_{gas}(X)$ gas- and $E_{aq}(X)$ condensed-phase electronic energies evaluated at the corresponding optimized geometries, respectively. $G_{CDS}(X)$ is the free enegy change associated with solvent cavitation (C), change in dispersion (D) and local solvent structure (S). ΔG^0_{add} in Eq. (4) is the Gibbs energy contribution of -1.9 kcal/mol required for the transfer of the molecule from the standard gas phase of 1 atm pressure to the standard solution state of 1 mol/L.[54,55] In the case of the *Imp-Exp* approach for condensed phase (see Figure 2b) the concentration of the water was supposed to be 55.34 mol/L, thus a contribution of $RT \ln[\mathrm{H_2O}] = 2.38$ kcal/mol was added to the Gibbs energy of the pure water. This correction was also taken into account at the calculation of the Gibbs energy of the complexation reaction, $\Delta_r G^0_{aq,complex}$ (Figure 2c). Since the gas-phase Gibbs energy and the Gibbs energy of solvation of the proton cannot be determined accurately with

theoretical methods,[56] the experimental values of -6.28 kcal/mol and -265.9 kcal/mol were taken for $G^0_{gas}(\mathrm{H}^+)$ and $\Delta_{solv}G^0(\mathrm{H}^+)$, respectively.[57]

The enthalpy and entropy of the ground- and excited-state species were computed at the corresponding optimized geometries in the gas phase. The calculations were carried out using the rigid rotor-harmonic oscillator approximation supposing that the temperature is 298.15 K and the pressure is 1 atm. For the excited states the *eq* solvation of the LR-CPCM model was employed because analytic derivatives are not available for the SS-CPCM approach. For the gas-phase water complexes and protonated coumarins the basis set superposition error (BSSE) was corrected with the counterpoise (CP) method,[58,59] but no attempt was made to apply the CP method in the solution phase. At the calculation of Gibbs energies of solvation the uncorrected energies were consider also for the gas-phase species to be consistent with the energies obtained for the condensed-phase molecules.

3. RESULTS AND DISCUSSION

3. 1. Structure and stability of C102-water complexes

The ground and excited state optimized geometries of the neutral molecule, the protonated species and the water complexes are presented in Table S1 of the Supporting Information (SI). The structure of the coumarin skeleton changes only slightly upon excitation for all the studied species, its quasi-planar structure is preserved. Notable changes can only be observed for the hydrogen bond lengths of the two water complexes (see Table 1). For the the amino complex, $\mathrm{C_N}\cdots\mathrm{H_2O}$, the length of the hydrogen bond is 2.050 Å in the S_0 state, but after the excitation the hydrogen bond is broken. In the oxo complex, $\mathrm{C_O}\cdots\mathrm{H_2O}$, the hydrogen bond connected to the carbonyl group shortens by 0.052 Å in the excited state, while the length of the H—O bond between the hydrogen atoms forming the hydrogen bond and the oxygen of the water molecule increases from 0.976 Å to 0.981 Å. We note that we also studied a complex where the water molecule is hydrogen bonded to the ether oxygen, however, during the geometry optimizations the water molecule always reoriented to the oxo group. We also note that there exists another orientation of the water molecule relative to the carbonyl group – in which the O_{ring}–C=O···HOH chain of atoms have a *cis* arrangement, in contrast to their *trans* arrangement in the structure

shown in Fig 1. The *cis* conformer is very close in energy to the *trans* one we considered in our calculations. In the ground state the *cis*, whereas in the excited state the *trans* complex is the lower energy conformer. The pK_a^* for the *cis* conformer is closer to the experimental value by 0.2 units. Since this difference is significantly smaller than the entire error with respect to the experiment, we present here the results only for the *trans* conformer.

Table 1. Hydrogen bond lengths [r(H···X)] and Gibbs energies of hydrogen bonding $\left(\Delta_r G^0_{aq,complex}\right)$ for C102-water complexes.

	S_0		S_1	
Complex	r(H···X) (Å)	$\Delta_r G^0_{aq,complex}$ (kcal/mol)	r(H····X) (Å)	$\Delta_r G^0_{aq,complex}$ (kcal/mol)
$\left[C_N \cdots H_2O\right]_{aq}$	2.050	3.5	-	-
$\left[C_O \cdots H_2O\right]_{aq}$	1.808	1.6	1.756	1.0

The hydrogen bond at the amino site is already weaker in the ground state than at the oxo site, and after the excitation, which is accompanied by a significant charge transfer, the hydrogen bond of the amino complex is broken, while that of the oxo complex strengthens. According to the $\Delta_r G^0_{aq,complex}$ value for the S_0 state in Table 1, ~ 80 % of C102 is present in form of $C_O \cdots H_2O$ water complex in the neutral aqueous solution of the dye. The significant weakening of the amino complex and the strengthening of the oxo complex is in accordance with previous findings, though in other theoretical studies on C102[60] and similar molecules[61] weak complexes were reported also in the S_1 state with very long hydrogen bonds.

3. 2. Absorption and emission spectra

The absorption and fluorescence spectra of C102 recorded at different pH values are displayed in Figure 3. The latter are 'normalized spectra', i. e. they have been corrected by the spectral sensitivity of the instrument and have been normalized by the absorbance values at the excitation

wavelength. The fluorescence spectra have also been corrected for the inner filter effect by using the approximate formula[62]

$$I^{corr} = I^{measd} \times 10^{[(A_{exc} - A_{em})/2]}, \qquad (6)$$

where A_{exc} and A_{em} are the absorbance values at the excitation and emission wavelengths, respectively.

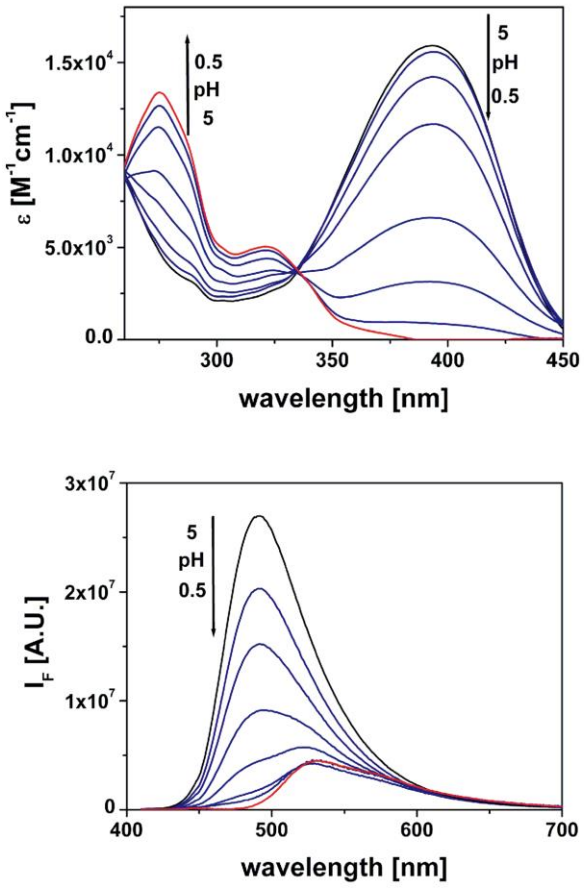

Figure 3. Absorption and fluorescence spectra of C102 measured in acidic aqueous solutions. The red traces are the spectra of protonated C102 obtained by least square fitting.

It has been checked that the spectra obtained in neat water, in basic solution (0.1 M NaOH) and in weakly acidic solutions upto pH = 5 were identical, thus these spectra were taken as the spectra of the C102 base. The absorption and fluorescence spectra of protonated C102, together with the equilibrium constants for the protonation of C102 in its ground and excited states, K_{pr} and K_{pr}^{*}, were obtained from the respective pH dependent experimental spectra by a least square fitting calculation. (Details of the fitting are given in SI). The values of the equilibrium constants

obtained were K_{pr} = 40.5 M^{-1} and K^*_{pr} = 155 M^{-1}, corresponding to pK_a = 1.61 and pK^*_a = 2.19, respectively. It has to be emphasized that the latter value can be considered a true equilibrium constant only if the equilibrium is reached well within the lifetimes of excited state C102 and its protonated form. The fulfillment of this condition will be discussed in section 3.4. The ratio of the fluorescence quantum yields of the neutral and protonated solutes obtained as the ratio of the respective integrated emission intensities, is 4.7. Using the value of Φ^F = 0.66 for C102 in aqueous solution,[63] the value of Φ^F = 0.14 is obtained for the protonated dye.

Table 2. Wavelengths of the visible absorption and fluorescence bands (λ^{abs}_{max} and λ^{F}_{max}) in the experimental and calculated spectra of unprotonated (C) and protonated C102 (CH^+). The intensities are given as absorption coefficients (ε_{max}) and fluorescence quantum yields (Φ^F) in the experimental spectra, as oscillatory strengths (f^{abs}, f^F) in the calculated spectra.

Experimental					Calculated				
Solute	λ^{abs}_{max} (nm)	ε_{max} ($M^{-1}cm^{-1}$)	λ^{F}_{max} (nm)	ϕ^F	Solute	λ^{abs}_{max} (nm)	f^{abs}	λ^{F}_{max} (nm)	f^F
C	393	16.5×10^3	493	0.66[a]	C_{aq}	412	0.359	480	0.352
					$[C_N\cdots H_2O]_{aq}$	400	0.353	-	-
					$[C_O\cdots H_2O]_{aq}$	414	0.375	481	0.352
CH^+	321	5×10^3	532	0.14	$C_NH^+_{aq}$	342	0.062	519	0.049
					$C_OH^+_{aq}$	408	0.310	500	0.217

[a] from Ref. [63]

The experimental and the theoretically calculated absorption and emission spectra of the neutral species are shown in Figure 4, while those for the protonated coumarins are displayed in Fig. 5. The transition wavelengths and probabilities for the $S_0 \rightarrow S_1$ transition are compiled in Table 2. In general, we can conclude that the agreement of the theoretical and experimental

excitation energies is good (error of about 0.1 eV), and even the significant Stokes shift peculiar to the coumarins is also well reproduced (error of about 0.15 eV). The good agreement can be attributed to the carefully parametrized SMD solvation model and the SS approach. We note that using other solvation schemes we obtained less satisfactory results.

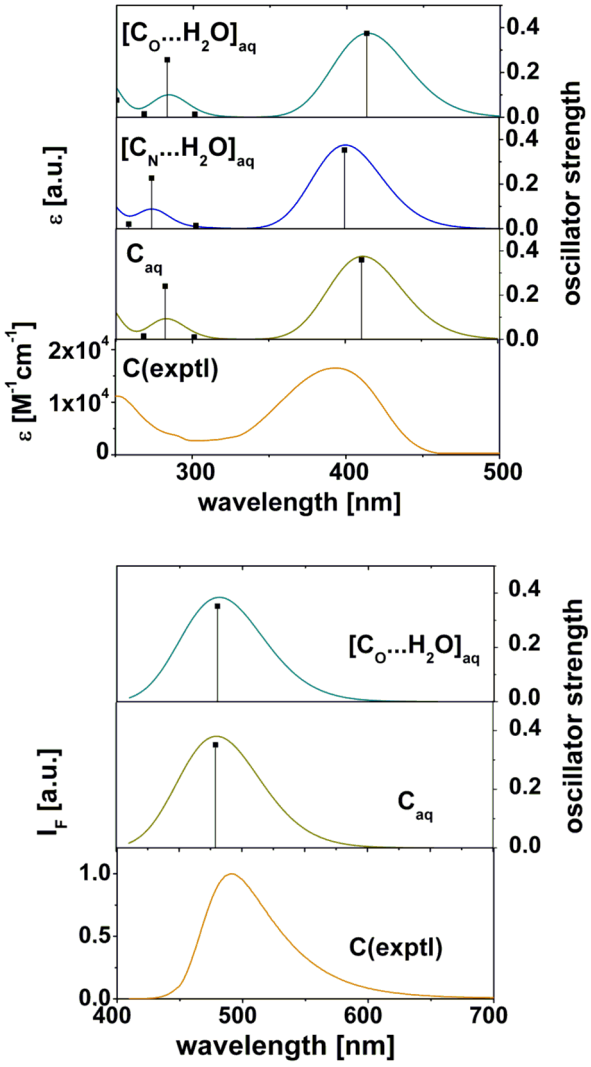

Figure 4. Experimental and calculated absorption (top) and fluorescence (below) spectra of C102 (C) in aqueous solution.

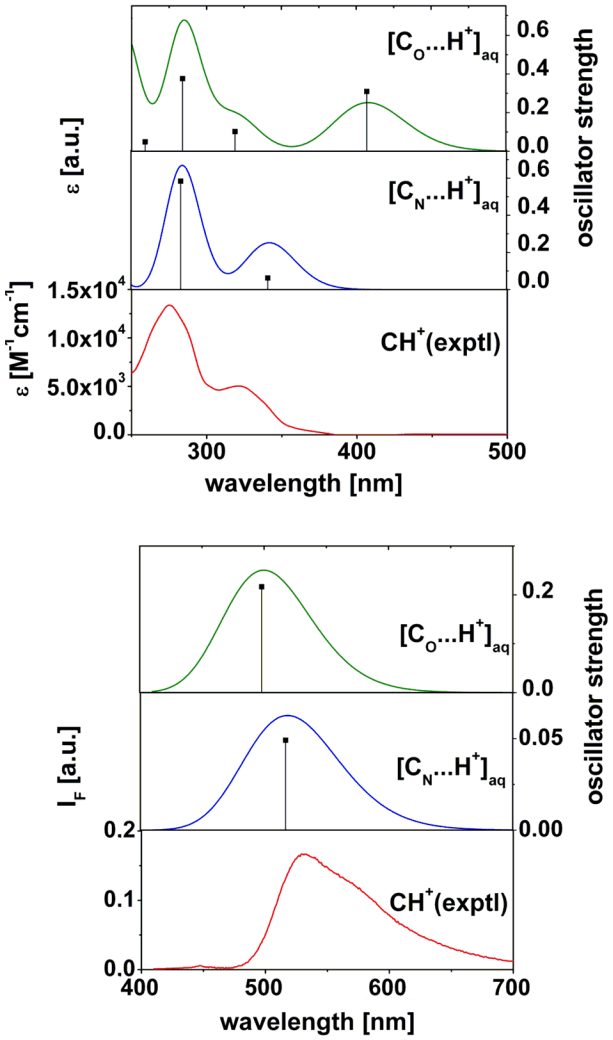

Figure 5. Experimental and calculated absorption (top) and fluorescence (below) spectra of protonated C102 (CH^+) in aqueous solution.

The $S_0 \rightarrow S_1$ transition of the neutral species is dominated by the HOMO → LUMO excitation and is of $\pi \rightarrow \pi^*$ character. The explicit solvent molecule only moderately influences the spectrum, but it can be seen that both the absorption and fluorescence spectrum of the oxo complex $C_O\cdots H_2O$ are slightly shifted to the red, while those for the amino complex $C_N\cdots H_2O$ are somewhat blueshifted with respect to the free dye. The $S_0 \rightarrow S_1$ transition of the protonated forms is also dominated by the HOMO → LUMO excitation, but the HOMO-1 → LUMO (for species C_OH^+) and the HOMO-1 → LUMO+1 (for species C_NH^+) excitations, which are also of $\pi \rightarrow \pi^*$ character, also considerably contribute. The $S_0 \rightarrow S_1$ transition of the latter species is of

low oscillator strength, the 275 nm peak of the experimental absorption spectrum is assigned to the $S_0 \rightarrow S_2$ transition, whose calculated absorption wavelength is 284 nm. On the basis of the characteristic features of the absorption spectra the protonation site in ground state can be unequivocally identified. In the computed spectrum of C_OH^+ an intense band redshifted with respect to the neutral solute appears which is missing from the spectrum recorded in acidic solution. In turn, the blueshifted spectrum of C_NH^+ agrees well with the experimental one. Concerning the $S_1 \rightarrow S_0$ emission transition of the protonated coumarins we observe that its character for C_NH^+ somewhat changes with respect to that of the $S_0 \rightarrow S_1$ absorption and is dominated by the LUMO → HOMO transition, while for C_OH^+ both the LUMO → HOMO and LUMO → HOMO-1 transitions still have major contributions. The fluorescence spectrum of both protonated species is shifted to the red with respect to the parent C102, though for C_NH^+ the probability of the transition, similarly to the absorption, is low. Thus, the comparison of the theoretical and measured emission spectra alone does not help us to identify where the protonation takes place in the acidic solution.

3. 3. Calculation of pK_a and pK_a^*

The pK_a and pK_a^* values obtained using the thermodynamic and Förster cycles are collected in Table 3. As discussed before, a comparison of the experimental ground and excited absorption spectra indicates that the protonation on the amino group is preferred in the ground state. The theoretical pK_a values computed applying the thermodynamic cycle confirm this result: the pK_a for the protonation of the amino group are larger by 4.54 units (*Imp* solvent model) or 5.89 units (using the *Imp-Exp* model) than the respective figures for the protonation of the carbonyl group. The best agreement with the experiment is achieved with the *Imp-Exp* approach, for which the difference with respect to the experiment is only 0.60, which is decreased further to 0.19 using the BSSE correction. It is also obvious that the addition of the explicit solvent molecule significantly, by 2.68 units improves the description of the system. All in all, the comparison of the computed and measured pK_a-s supports the conclusions of the spectrum calculations, that is, in the ground state the basicity of the amino group is much higher than that of the carbonyl group.

Table 3. pK_a and pK_a^* from the thermodynamic and Förster cycles for the various protonation sites. The BSSE-corrected thermodynamic cycle results are given in parentheses.

		Thermodynamic cycle		Förster cycle
Protonation site	Solvent model	pK_a	pK_a^*	pK_a^*
NH^+	*Imp*	-1.67 (-2.14)	-11.98 (-12.45)	-2.16
	Imp-Exp	1.01 (1.42)	-	-
OH^+	*Imp*	-6.21 (-6.37)	-1.28 (-1.44)	2.28
	Imp-Exp	-4.88 (-4.65)	-0.41 (0.27)	2.06
exptl.		1.61	2.19	2.19

In the excited state no definitive conclusion can be drawn concerning the preferred protonation site of C102 on the basis of the emission spectra, thus the inspection of the computed pK_a^* values are even more interesting (see column 4 in Table 3). Here the reference value is the experimental pK_a^* again, which is 2.19. The results show that in the excited state the oxo group is definitely more basic since the difference in the pK_a^* values calculated for the oxo and amino protonation is more than 10 units. Again, the best performance is observed for the *Imp-Exp* approximation, though its error is remarkably larger, about 2.6 units, which is, however, improved by 0.68 units when adding the BSSE correction. The inaccuracy of the *Imp-Exp* method is also shown by the fact that the experimental pK_a difference between the ground and excited states of 0.58 unit is not reproduced, in contrast, a pK_a drop of 1.42 (from 1.01 to -0.41) is predicted. On the other hand, though the *Imp* approach (*Imp* approach with BSSE correction) underestimates the experimental values in average by 3.47 (3.63) pK_a units, it correctly distinguishes between the protonation sites, and estimates the experimental pK_a change of 0.58 unit relatively well as 0.39 (0.70). In conclusion, from the pK_a^* values obtained with the thermodynamic cycle we can

deduce that the basicities of the amino and oxo groups remarkably change due to the electronic excitation, and the oxo group becomes more basic in the S_1 state.

We note in passing that the effect of the BSSE is usually ignored in pK_a or pK_a^* calculations.[48,50] Our results show that the BSSE correction calculated with the CP method to the pK_a and pK_a^* values is considerable, about 0.5 units, though, in the case of pK_a^* it is significantly smaller than the entire error with respect to the experiment. Thus, the consideration of basis set effects is recommended in pK_a calculations, though probably an improved correction instead of the CP method should be used.[64]

The results of the Förster-cycle relying on transition energies are in good agreement with the above findings (see the rightmost column in Table 3). This simplistic model successfully determines the site of the excited-state protonation: the pK_a^* value predicted for the amino group is by more than 4 units larger than that for the oxo group. The pK_a^* values computed either by the *Imp* or by the *Imp-Exp* models agree surprisingly well with the experimental ones, especially in comparison to the results of the thermodynamic cycle. This can partly be explained by the relatively high accuracy of the excitation energies computed with the SS approach, but a considerable benefit from fortunate error cancellation is also likely.

3.4. Kinetic analysis

Fluorescence decay curves were measured of samples with pH values between 0.5 and 3 and in neat water at two emission wavelengths: at 465 nm, where only the emission of the unprotonated form is detectable, and at 625 nm, where the protonated form is the dominant emitter, at least below pH 2.5. At the wavelength of the excitation laser, 378 nm, the absorption of the neutral form dominates.

The evaluation of the individual decay curves is described in SI. Here we present a more complex evaluation, a kind of global analysis of all decay curves (measured at both wavelengths at various pH values) based on a model with just 3 adjustable parameters (rate constants) – the feasibility of such an evaluation greatly increases the credibility of the model applied.

In order to enable such an evaluation we had to perform the measurements in a special way: the decay curves of a given sample measured at the two selected wavelengths were collected with identical excitation laser intensities and the time needed for data collection has been

recorded as well. In this way we were able to resolve the emission intensities into the contributions of the individual species (neutral and protonated C102) from the data using the formulae

$$I^{n}_{465} = I^{meas}_{465}/\beta_{465}, \tag{7}$$

and

$$I^{pr}_{625} = I^{meas}_{625}/\beta_{625} - I^{n}_{625} = I^{meas}_{625}/\beta_{625} - \left(I^{meas}_{465}/\beta_{465}\right)\left(I^{n,st}_{625}/I^{n,st}_{465}\right)\left(t^{coll}_{625}/t^{coll}_{465}\right), \tag{8}$$

respectively, where I^{meas}_{λ} is the measured intensity, β_{λ} is the sensitivity in the detection arm of the single-photon counting system, $I^{n,st}_{\lambda}$ is the intensity in the stationary spectrum and t^{coll}_{λ} is the data collection time at λ nm. (As the overall emissions of the samples with different pH values were much weaker at 625 nm than at 465 nm, to obtain decay curves with similarly high S/N ratios at the two wavelengths, the decays at 625 nm were recorded applying much longer data collection times.)

Repeated application of Eq. (7) and (8) at each pH and at each time delay yielded the decay profiles of both species for all pH values. As an example, Figure 6 shows the decay curves for the sample of pH = 1.5, measured at 465 and 625 nm, together with the calculated I^{pr}_{625} values. As can be seen, the emission of protonated C102 builds up within the first ns after the excitation pulse.

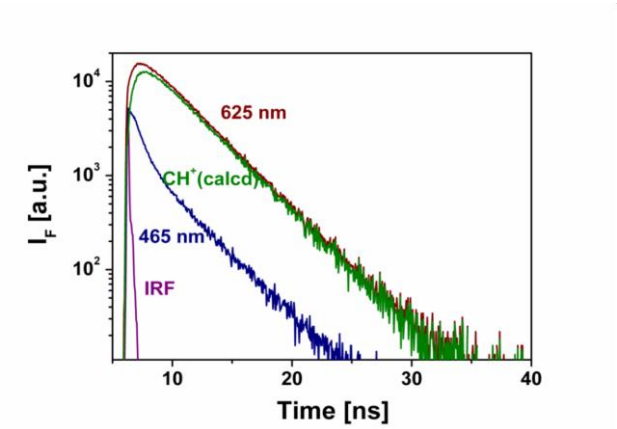

Figure 6. Fluorescence decay curves measured at λ_{em} = 465 and 625 nm in pH 1.5 solution (λ_{ex} = 378 nm, the curves are corrected for spectral sensitivity of the emission arm), the instrument response function (IRF) and the calculated emission from protonated C102.

The time profiles of the two excited species were calculated with help of the fourth order Runge-Kutta integration formulae, using the following set of chemical reactions and rate coefficients:

$$C + h\nu \rightarrow C^* \qquad (9)$$

$$CH^+ + h\nu \rightarrow CH^{+*} \qquad (10)$$

$$C^* \rightarrow C(+h\nu') \qquad k_{dec}^{n}(ns^{-1}) \qquad (11)$$

$$C^* + H^+ \rightarrow CH^{+*} \qquad k_{pr}(M^{-1}ns^{-1}) \qquad (12)$$

$$CH^{+*} \rightarrow C^* + H^+ \qquad k_{dpr}(ns^{-1}) \qquad (13)$$

$$CH^{+^*} \rightarrow C + H^+ \text{ or } CH^+(+h\nu''), \quad k_{dec}^{pr}(ns^{-1}) \qquad (14)$$

where C^* and CH^{+*} stand for the excited species. The ground state equilibrium constant between neutral and protonated C102 has been determined as 40.5 M^{-1}, thus the ratio of the neutral and protonated C102 concentration is known at each pH. Since the hydroxonium ion concentration is higher by several orders of magnitude even under the least acidic conditions, as compared to the concentration of the excited dye, it can be treated as constant, thus $k_{pr} \cdot [H^+]$, measured in ns^{-1} can be used for the kinetic description of reaction (12), thus all interactions can be modeled as first-order reactions. The symbols in parenthesis, hν' and hν'' mean that the corresponding rate coefficients represent all decay channels of the corresponding species, including fluorescence, through which we detect these species; ν' includes both 465 nm and 625 nm (with relative weights $I_{625}^{n,st}/I_{465}^{n,st}$), while ν'' does not include 465 nm, only 625 nm. The rates of reactions (9) and (10) are proportional to the time-profile of the excitation laser pulse (which was measured separately in the usual way using a light scattering sample). The molar absorption coefficients of the two forms were known at the wavelength of the excitation laser, 378 nm (15200 $M^{-1}cm^{-1}$ for neutral and 190 $M^{-1}cm^{-1}$ for protonated C102), thus the direct excitation of both forms could be modeled.

The time-dependent modeled emission intensities from both excited species at various pH values between 1.0 and 3.0 were built up by a numerical integration and were fitted to the experimental decay curves using k_{pr}, k_{dpr} and k_{dec}^{pr} as fitting parameters.

Table 4. Rate coefficients for the deactivation of neutral and protonated C102 (k_{dec}^{n} and k_{dec}^{pr}), for excited state protonation of C102 (k_{pr}) and the reverse reaction (k_{dpr}).

Parameter	Data sets (pH values) used for estimation	Parameter value
k_{dec}^{n} (s^{-1})	no additive, ~7	$1.67_4 \times 10^8$
k_{dec}^{pr} (s^{-1})	1.0 – 3.0	3.27×10^8
k_{pr} ($M^{-1}s^{-1}$)	1.0 – 3.0	3.27×10^{10}
k_{dpr} (s^{-1})	1.0 – 3.0	2.78×10^8

The results of the parameter estimation are summarized in Table 4, while the excellent goodness of fit can be seen in Table S3 in SI. The almost even spread of squared residuals testifies that the model and its parameters adequately describe all decays at all pH values. In Figure. 7 the calculated decay profiles are shown only for the intervals, which have been taken into account during parameter estimation.

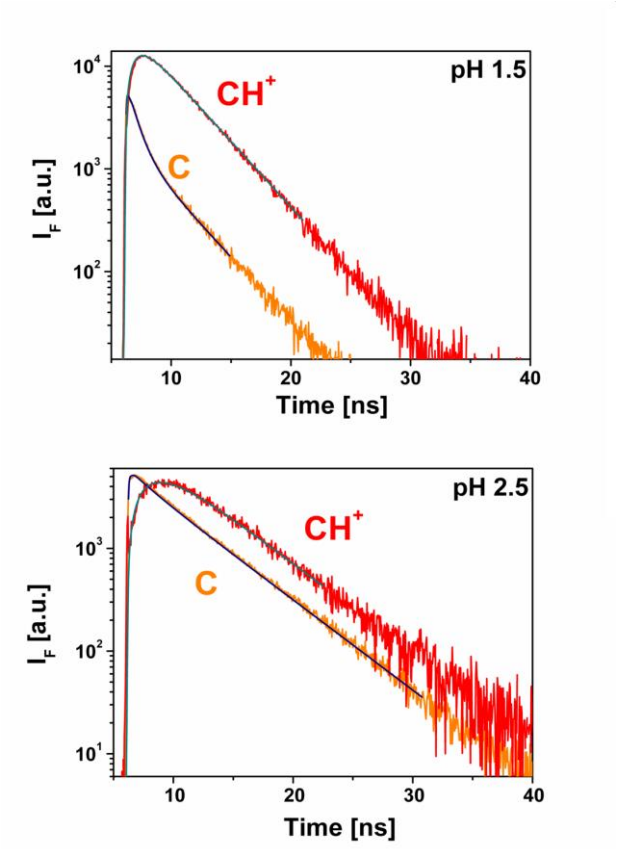

Figure 7. Calculated fluorescence decay profiles of neutral and protonated Coumarin 102 at pH = 1.5 (top) and 2.5 (below). The fitted functions are shown as smooth lines.

From the values of k_{pr} and k_{dpr} in Table 4, which were taken independent parameters in this kinetic analysis, K_{pr}^{*} = 117 M^{-1} was obtained, showing a good agreement with K_{pr}^{*} = 155 M^{-1} calculated from the stationary fluorescence spectra. A more established way to judge how much the equilibrium state is approached, is to compare $k_{pr}\left[H^{+}\right]+k_{dpr}$, the rate coefficient of protonation/deprotonation as a quasi first order equilibrium reaction, to k_{dec}^{n} and k_{dec}^{pr}, the rate coefficients associated with the deactivation processes of the two excited state species. Taking the respective values from Table 4, one can conclude that the condition $k_{pr}\left[H^{+}\right]+k_{dpr} > k_{dec}^{n}, k_{dec}^{pr}$ is fulfilled, i.e. the system can be considered as quasi-equilibrium in strongly acidic (pH ≤ 2) media. This can be seen from Figure 7: at pH 1.5 the decays of C^{*} and CH^{+*} run parallel from ~5 ns following the excitation whereas at pH 2.5 this time is ~10 ns.

4. CONCLUSIONS

The purpose of this combined spectroscopic and theoretical study was to reveal the effects of complexation and protonation of C102 on its spectral properties. The employed (TD)DFT methods together with the CPCM/SMD solvation model, especially with the SS formalism, turned out to be excellent tools for the simulation of absorption and fluorescence spectra. The computed absorption spectra were in good agreement with the experimental ones, and they allowed us to conclude that the molecule is protonated on the amino group in its ground state. This observation is also born out by our pK_a values obtained with the thermodynamic cycle approach. We have found that the complexation only slightly influences the spectra, the hydrogen bond formation at the amino group results in a moderate blue shift of the spectra, while that for the oxo group has the opposite effect. The electronic excitation results in a significant transfer of electron density from the direction of the amino group towards the oxo group, and the hydrogen bond of the amino-complex breaks, while that of the oxo-complex strengthens. Parallel to that process the basicity of the carbonyl group increases with respect to the amino group, which was also verified by the calculation of the relevant logarithmic acid dissociation constants via thermodynamic cycles. The pK_a^* values were also computed with the aid of the Förster-cycle, which, in spite of its simplicity, provides good estimates for those quantities. We also note that the computational protocol employed in this study may be useful for the calculation of pK_a^* values for similar excited states, especially when the experimental pK_a^* measurements are not possible.

As the low values obtained for the ground and excited state protonation equilibrium constants (pK_a = 1.61, pK_a^* = 2.19) for C102 show, the protonations of the ground as well as the excited state dye molecules are not significant in neutral or weakly acidic media, occurring in the great majority of pharmacokinetic and biochemical applications of this fluorescent probe. On the other hand, the relatively high fluorescence quantum yield and the large Stokes shift of its protonated form make this compound an attractive fluorescent probe also for more acidic environments, occurring e.g. in proton transfer membranes. However, as the results of the kinetic analysis showed, the evaluation of the fluorescence data obtained with this dye in such media is rather

complex, even in homogenous aqueous solutions, in particular in a pH range (2 < pH < 3) where the rates of the decays of the neutral and the protonated forms, and the rate of the protonation of the excited dye, which is a reversible reaction, are commeasurable, thus, the two emissive species are not in equilibrium. From the equilibrium constants and photophysical data determined in this study, the stationary and time-resolved fluorescence spectra of this dye probe can be calculated as a function of pH and excitation wavelength.

ASSOCIATED CONTENT

Supporting Information. Cartesian coordinates of C102, its protonated forms and water complexes. Calculation of pK_a and absorption spectrum of protonated C102. Calculation of pK_a^* and fluorescence spectrum of protonated C102. Semi-quantitative analysis of individual decay data. Comments to the detailed analysis of decay data. This material is available free of charge via the Internet at http://pubs.acs.org.

AUTHOR INFORMATION

Corresponding Author

*E-mail: kubinyi@mail.bme.hu

ACKNOWLEDGMENT

The authors are grateful for the financial support from the Hungarian Scientific Research Fund (OTKA, Grant No. K108752).

References

[1] Wagner, B. D. The Use of Coumarins as Environmentally-Sensitive Fluorescent Probes of Heterogeneous Inclusion systems. *Molecules* **2009**, *14*, 210-237.

[2] Haidekker, M.A.; Brady, T. P.; Lichlyter, D.; Theodorakis, E. A. Effects of Solvent Polarity and Solvent Viscosity on the Fluorescent Properties of Molecular Rotors and Related Probes. *Bioorg. Chem.* **2005**, *33,* 415-426.

[3] Bank, A.; Kumbhakar, M.; Nath, S.; Pal, H. Evidence for the TICT Mediated Nonradiative Deexcitation Process for the Excited Coumarin-1 Dye in High Polarity Protic Solvents. *Chem. Phys.* **2005**, *315*, 277-285.

[4] Grant, C. D.; Steege, K. E.; Bunagan, M. R.; Castner Jr., E. W. Microviscosity in Multiple Regions of Complex Aqueous Solutions of Poly(ethylene oxide)-poly(propylene oxide)-poly(ethylene oxide) *J. Phys. Chem. B* **2005**, *109*, 22273-22284.

[5] Bhattacharya, B.; Nakka, S.; Guruprasad, L.; Samanta, A. Interaction of Bovine Serum Albumin with Dipolar Molecules: Fluorescence and Molecular Docking Studies. *J. Phys. Chem. B* **2009**, *113*, 2143–2150.

[6] Patra, S.; Santhosh, K., Pabbathi, A.; Samanta, A. Diffusion of Organic Dyes in Bovine Serum Albumin Solution Studied by Fluorescence Correlation Spectroscopy. *RSC Advances*, **2012**, *2*, 6079–6086.

[7] Frauchiger, L.; Shirota, H.;. Uhrich, K.E.; Castner, Jr., E. W. Dynamic Fluorescence Probing of the Local Environments within Amphiphilic Starlike Macromolecules. *J. Phys. Chem. B* **2002**, *106*, 7463-7468.

[8] Lee, H.-i.; Wu, W.; Oh, J. K.; Mueller, L.; Sherwood, G.; Peteanu, L.; Kowalewski, T.; Matyjaszewski, K. Light-Induced Reversible Formation of Polymeric Micelles. *Angew. Chem. Int. Ed.* **2007**, *46*, 2453 –2457.

[9] Lee, J.-E.; Ahn, E.; Bak, J. M.; Jungd, S.-H.; Park, J. M.; Kim, B.-S.; Lee, H.-I. Polymeric Micelles Based on Photocleavable Linkers Tethered with a Model Drug. *Polymer* **2014**, *55*, 1436-1442.

[10] Halder, A.; Sen, S.; Burman, A. Das; Patra, A.; Bhattacharyya, K. Solvation Dynamics in Dimyristoyl-Phosphatidylcholine Entrapped Inside a Sol−Gel Matrix. *J. Phys. Chem. B* **2004**, *108*, 2309-2312.

[11] Lim, L. H.; Tan, A.; Simovic, S.; Prestidge, C. A. Silica-lipid Hybrid Microcapsules: Influence of Lipid and Emulsifier Type on in Vitro Performance. *Int. J. Pharm*. **2011**, *409*, 297–306.

[12] Zhang, J.; Ma, P. X. Polymeric Core–Shell Assemblies Mediated by Host–Guest Interactions: Versatile Nanocarriers for Drug Delivery. *Angew. Chem. Int. Ed.* **2009**, *48*, 964 – 968.

[13] Somoza, M. M.; Andreatta, D.; Murphy, C. J.; Coleman, R. S.; Berg, M. A. Effect of Lesions on the Dynamics of DNA on the Picosecond and Nanosecond Timescales Using a Polarity Sensitive Probe. *Nucleic Acids Res.* **2004**, 32, 2494-2507.

[14] Coleman, R. S.; Berg, M. A.; Murphy, C. J. Coumarin Base-Pair Replacement as a Fluorescent Probe of Ultrafast DNA Dynamics. *Tetrahedron* **2007**, *63*, 3450–3456.

[15] Burai, T. N.; Datta, A. Slow Solvation Dynamics in the Microheterogeneous Water Channels of Nafion Membranes. *J. Phys. Chem. B* **2009**, *113*, 15901-15906.

[16] Iyer, E. S. S.; Datta, A. Importance of Electrostatic Interactions in The Mobility of Cations in Nafion. *J. Phys. Chem. B* **2011**, *115*, 8707–8712.

[17] Dey, A.; Patwari, G. N. Estimation of Interfacial Acidity of Sodium Dodecyl Sulfate Micelles. *J. Chem. Sci.* **2011**, *123*, 909-918.

[18] Molotsky, T.; Huppert, D. Site Specific Solvation Statics and Dynamics of Coumarin Dyes in Hexane−Methanol Mixture. *J. Phys. Chem. A* **2003** ,*107*, 2769-2780.

[19] Liu, Y.-H.; Li, P. Excited-State Hydrogen Bonding Effect on Dynamic Fluorescence of Coumarin 102 Chromophore in Solution: A Time-Resolved Fluorescence and Theoretical Study. *J. Lumin.* **2011**, *131*, 2116–2120.

[20] Barman, N.; Singha, D.; Sahu, K. Fluorescence Quenching of Hydrogen-Bonded Coumarin 102-Phenol Complex: Effect of Excited-State Hydrogen Bonding Strength. *J. Phys. Chem. A* **2013**, *117*, 3945-3953.

[21] Moog, R. S.; Bankert, D. L.; Maroncelli, M. Rotational Diffusion of Coumarin 102 in Trifluoroethanol: the Case for Solvent Attachment. *J. Phys. Chem.* **1993**, *97*, 1496-1501.

[22] Chudoba, C.; Nibbering, E. T. J.; Elsaesser, T. J. Ultrafast Structural Response of Hydrogen Bonded Complexes to Electronic Excitation in the Liquid Phase. *J. Phys. Chem. A* **1999**, *103*, 5625-5628.

[23] Nibbering, E. T. J.; Tschirschwitz, F.; Chudoba, C.; Elsaesser, T. Femtochemistry of Hydrogen Bonded Complexes after Electronic Excitation in the Liquid Phase: The Case of Coumarin 102. *J. Phys. Chem. A* **2000**, *104*, 4236-4246.

[24] Palit, D. K.; Zhang, T.; Kumazaki, S.; Yoshihara, K. Hydrogen-Bond Dynamics in the Excited State of Coumarin 102−Aniline Hydrogen-Bonded Complex. *J. Phys. Chem. A* **2003**, *107*, 10798-10804.

[25] Wells, N. P.; McGrath, M. J.; Siepmann, J. I.; Underwood, D. F.; Blank, D. A. Excited State Hydrogen Bond Dynamics: Coumarin 102 in Acetonitrile−Water Binary Mixtures. *J. Phys. Chem. A* **2008**, *112*, 2511-2514.

[26] Zhao, G.-J.; Han, K.-L.; Early Time Hydrogen-Bonding Dynamics of Photoexcited Coumarin 102 in Hydrogen-Donating Solvents: Theoretical Study. *J. Phys. Chem. A* **2007**, *111*, 2469-2474.

[27] Liu, Y. F.; Ding, J. X.; Shi, D. H.; Sun, J. F. Time-Dependent Density Functional Theory Study on Electronically Excited States of Coumarin 102 Chromophore in Aniline Solvent: Reconsideration of the Electronic Excited-State Hydrogen-Bonding Dynamics. *J. Phys. Chem. A* **2008**, *112*, 6244-6248.

[28] Su, J.; Tian, D. Strengthening of Hydrogen Bonded Coumarin 102 in Ethanol Solvent upon Photoexcitation. *New J. Chem*. **2014**, *38*, 568-573.

[29] Miao, C.; Shi, Y. Reconsideration on Hydrogen Bond Strengthening or Cleavage of Photoexcited Coumarin 102 in Aqueous Solvent: A DFT/TDDFT Study. *J. Comput. Chem.* **2011**, *32*, 3058-3061.

[30] Campillo, A. J.; Clark, J. H.; Shapiro, S. L.; Winn, K. R.; Woodbridge, P. K. Excited-State Protonation Kinetics of Coumarin 102. *Chem. Phys. Lett.* **1979**, *67*, 218- 222.

[31] Bursulaya, B. D.; Druzhinin, S. I.; Uzhinov, B. M. J. Fast Dynamic Excited State Proton Transfer (ESPT) Reaction of Weak Oxoaromatic Bases. Aminocoumarins with Fixed Amino Group. *J. Photochem. Photobiol. A: Chemistry* **1995**, *92*, 163-172.

[32] Grabowski, Z. R.; Rotkiewicz, K.; Rettig, W. Structural Changes Accompanying Intramolecular Electron Transfer: Focus of Twisted Intramolecular Charge Transfer States and Structures. *Chem. Rev*. **2003**, *103*, 3899-4031.

[33] Förster, T. Die pH-Abhängigkeit der Fluoreszenz von Naphthalinderivaten. *Z. Electrochem.* **1950**, *54*, 531-535.

[34] Born, M. Eine thermochemische Anwendung der Gittertheorie. *Ber. Physik.***1919**, *21*, 13-24.

[35] Haber, F. Betrachtungen zur Theorie der Wärmetönung. *Ber. Physik.* **1919**, *21,* 750-768.

[36] Pines, D.; Pines, E. Solvent Assisted Photoacidity in *Handbook of Hydrogen-Transfer Reactions Volume 1: Physical- and Chemical Aspects of Hydrogen Transfer*; Wiley-VCH, Weinheim, Germany, 2007

[37] Förster, T. Fluoreszenzspektrum und Wasserstoffionenkonzentration. *Naturwissenschaften* **1949**, *36*, 186-187.

[38] Houari, Y.; Jacquemin, D.; Laurent, A. TD-DFT Study of pK_a^* for Coumarins. *Chem. Phys. Lett.* **2013**, *583*, 218-221.

[39] Gaussian 09, Revision B.01, Frisch, M. J.; Trucks, G. W.; Schlegel, H. B.; Scuseria, G. E.; Robb, M. A.; Cheeseman, J. R.; Scalmani, G.; Barone, V.; Mennucci, B.; Petersson, G. A. *et al.* Gaussian, Inc., Wallingford CT, 2009

[40] Hohenberg, P.; Kohn, W. Inhomogenous Electron Gas. *Phys. Rev.* **1964**, *136*, B864-871.

[41] Kohn, W.; Sham, L. J. Self-Consistent Equations Including Exchange and Correlation Effects. *Phys. Rev.* **1965**, *140*, A1133-A1138.

[42] Adamo, C; Barone, V. Toward Reliable Density Functional Methods without Adjustable Parameters: The PBE0 Model. *J. Chem. Phys.* **1999**, *110*, 6158-6159.

[43] McLean, A. D.; Chandler, G. S. Contracted Gaussian Basis Sets for Molecular Calculations. I. Second Row Atoms, Z=11–18. *J. Chem. Phys.* **1980**, *72*, 5639-5648.

[44] Runge, E.; Gross, E. K. U. Density Functional Theory for Time-Dependent Systems. *Phys. Rev. Lett.* **1984**, *52*, 977-1000.

[45] Marenich, A. V.; Cramer, C. J.; Truhlar, D. G. Universal Solvation Model Based on Solute Electron Density and on a Continuum Model of the Solvent Defined by the Bulk Dielectric Constant and Atomic Surface Tensions. *J. Phys. Chem. B* **2009**, *113*, 6378-6396.

[46] Cossi, M.; Rega, N.; Scalmani, G.; Barone, V. Energies, Structures, and Electronic Propereties of Molecules in Solution with C-PCM Solvation Model. *J. Comput. Chem.* **2002**, *24*, 669-681.

[47] Barone, V.; Cossi, M. Quantum Calculations of Molecular Energies and Energy Gradients in Solution by a Conductor Solvent Model. *J. Phys. Chem. A* **1998**, *102*, 1995-2001.

[48] Jacquemin, D.; Perpéte, E. A.; Ciofini, I.; Adamo, C. Fast and Reliable Theoretical Determination of pK_a^* for Photoacids. *J. Phys. Chem. A* **2008**, *2*, 794-796.

[49] Lee, T. B.; McKee, M. L. Dependence of pK_a on Solute Cavity for Diprotic and Triprotic acids. *Phys. Chem. Chem. Phys.* **2011**, *13*, 10258-10269.

[50] Sutton, C. C. R.; Franks, G. V.; de Silva, G. First Principles pK_a Calculations on Carboxylic Acids Using the SMD Solvation Model: Effect of Thermodynamic Cycle, Model Chemistry and Explicit Solvation. *J. Chem. Phys. B* **2012**, *116*, 11999-12006.

[51] Cossi, M.; Barone, V. Solvent effect on Vertical Electronic Transitions by the Polarizable Continuum Model *J. Chem. Phys.* **2000**, *112*, 2427-2435.

[52] Improta, R.; Barone, V.; Scalmani, G.; Frisch, M. J. A State-Specific Polarizable Continuum Model Time Dependent Density Functional Theory Method for Excited State Calculations in Solution. *J. Chem. Phys.* **125** (2006) 054103.

[53] Cammi, R.; Mennucci, B. Linear Response Theory for the Polarizable Continuum Model. *J. Chem. Phys.* **1999**, *110*, 9877-9886.

[54] Ben-Naim, A. Standard Thermodynamics of Transfer. Uses and Misuses *J. Phys. Chem.* **1978**, *82*, 792-803.

[55] Ben-Naim, A.; Marcus, Y. Solvation Thermodynamics of Nonionic Solutes. *J. Chem. Phys.* **1984**, *81*, 2016-2027.

[56] Saracino, G.; Improta, R.; Barone, V. Absolute pK_a Determination for Carboxylic Acids Using Density Functional Theory and the Polarizable Continuum Model. *Chem. Phys. Lett.* **2003**, *373*, 411-415.

[57] Kelly, C. P.; Cramer, C. J.; Truhlar, D. G. Aqueous Solvation Free Energies of Ions and Ion-Water Cluster Based on an Accurate Value for the Absolute Aqueous Solvation Free Energy of the Proton. *J. Phys. Chem. B* **2006**, *110*, 16066-16081.

[58] Boys, S. F.; Bernardi, F. The Calculation of Small Molecular Interactions by the Differences of Separate Total Energies. Some Procedures with Reduced Errors. *Mol. Phys.* **1970**, *19*, 553-566.

[59] Simon, S.; Duran, M.; Dannenberg, J. J. How Does Basis Set Superposition Error Change the Potential Surfaces for Hydrogen−Bonded Dimers? *J. Chem. Phys. B* **1996**, *105*, 11024-11031.

[60] Zhao, W.; Ding, Y.; Xia, Q. Time Dependent Density Functional Study on the Absorption Spectrum of Coumarin 102 and its Hydrogen Bonded Complexes. *J. Comput. Chem.* **2010**, *32*, 545-553.

[61] Ramegowda, M. Change in Energy of Hydrogen Bonds Excitation of 6-aminocoumarin: TDDFT/EFP1 Study *New J. Chem.* **2013**, *37*, 2648-2653.

[62] Lakowicz, J. R. Principles of Fluorescence Spectroscopy; Kluwer: New York, 2006.

[63] Jones II, G.; Jackson, W. R.; Choi, C.-Y.; Bergmark, W. R. Solvent Effects on Emission Yield and Lifetime For Coumarin Laser Dyes. Requirements for a Rotatory Decay Mechanism. *J. Phys. Chem.* **1985**, *89*, 294-300.

[64] Mentel, Ł. M.; Baerends, E. J. Can the Counterpoise Correction for Basis Set Superposition Effect Be Justified? *J. Chem. Theory Comput.* **2014**, *10*, 252-267.

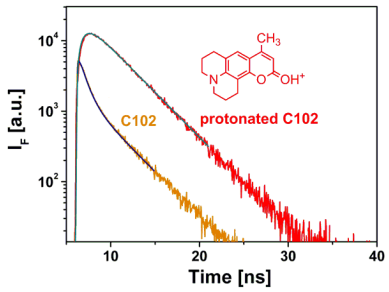

Table of Contents Image